REVISTA MATÉRIA
V.27 N.02
ISSN 1517-7076 artigo e13219, 2022

Processing of carbon-polymer porous composite from expanded graphite addition on poly(furfuryl alcohol)

Raissa Samira Rocha da Silva[1], Silvia Sizuka Oishi[1], Luiza dos Santos Conejo[2,3], Edson Cocchieri Botelho[2], Neidenêi Gomes Ferreira[1]

[1]Laboratório Associado de Sensores e Materiais, LABAS/INPE, Avenida dos Astronautas, 1758, Jardim da Granja, CEP: 12227-010, São José dos Campos, SP, Brasil
[2]Departamento de Materiais e Tecnologia, FEG/UNESP, Av. Dr. Ariberto Pereira da Cunha, 333, Pedregulho, CEP: 12516-410, Guaratinguetá, SP, Brasil
[3]Instituto de Pesquisa e Tecnologia, IPT/LEL, Estrada Dr. Altino Bondensan, 500, Distrito Eugênio de Melo, CEP: 12230-002, São José dos Campos, SP, Brasil
e-mail: raissamirarocha@gmail.com, silviaoishi@uol.com.br, luizaconejo@yahoo.com.br, edson.botelho@unesp.br, neidenei.ferreira@inpe.br

ABSTRACT

The addition of expanded graphite (EG) on environmentally friendly polymer matrix was systematically studied to produce carbon-polymer porous composite. Firstly, an appropriate EG was produced by monitoring the time and temperature of intercalated graphite thermal expansion while poly(furfuryl alcohol) (PFA) resin was obtained from the furfuryl alcohol polymerization. After PFA synthesis, different EG amounts of 0.2, 0.5, and 1.0 wt% were added in the resin and evaluated by viscosimetry and differential scanning calorimetry that showed EG helped in the crosslink formations decreasing the onset and endset temperatures. PFA resin kept a good fluidity, even for 1.0 wt% EG ensuring its homogeneous impregnation on the polyurethane foams. FTIR analyses confirmed the presence of functional groups on EG, which would contribute to the resin impregnation on the foam porous structure without changing the thermal resistance of the final product.

Keywords: Poly(furfuryl alcohol) resin, expanded graphite, porous composite, materials characterization.

1. INTRODUCTION

Considering the high demand for nanomaterials manipulation, carbon nanostructure represents an extremely attractive material due mainly to its high-performance for carbon-based devices not to mention its low cost and harmless behavior. Particularly, carbon/polymer composites have effectively been studied by combining their electrical and mechanical properties[1]. They are multi-phase materials, which associate polymer resins with reinforcing fillers by enhancing the composite properties due to the synergism between both their constituent materials. Also, carbon conducting fillers are very attractive mainly due to their low cost, high electrical conductivity, low density, and chemical stability. Thus, different fillers have been studied such as carbon nanotubes and graphite because of their ability to increase the mechanical, thermal, and electrical properties of native polymers [2-4].

Recently, P. Pokharel et al. have conducted a study related to how carbon nanomaterials can be combined with polymers to improve the mechanical and electrical properties of resultant composites [5]. They discussed the particle size and aspect ratio, filler morphology, and filler amounts as a conductive network in the polymer matrix. Besides, this composite synthesis demands a conductive nanofiller appropriate to the polymer matrix with a friendly interface between them. Therefore, graphite appears as a suitable filler not only due to its mechanical and electrical properties, but also to its easy processing. Nevertheless, for an efficient application, the graphite layers must be partially separated. These layers are separated by the addition of intercalants and give rise to the known intercalated graphite (IG) [6] which presents chemical groups increasing the chemical and/or physical interactions between the IG and the resin. Also, graphite as well as IG can be transformed into expanded graphite (EG) with an interlayered structure [7, 8], and its interlayer distance may be controlled by various methods [9]. NOH *et al.* [3] have compared the thermal conductivity of polymeric compounds filled with different carbon fillers such as carbon black, multi-wall carbon nanotubes,

Autor Responsável: Silvia Sizuka Oishi Data de envio: 16/06/2021 Data de aceite: 03/05/2022

10.1590/S1517-707620220002.1319

graphene nanoplatelets, graphite, carbon fibers, and EG [3, 7]. They concluded that EG was the most appropriate material for this study.

On the other hand, among several thermosetting resins available, the most used for the production of advanced carbonaceous materials are phenolic and poly(furfuryl alcohol) (PFA) resins. This is due to their high crosslink density when cured, as well as to their fixed carbon content of around 40% by mass. When compared to phenolic resins, PFA has some advantages: good mechanical and chemical resistance; possibility of a more controlled curing process, and mainly its production from renewable sources [10]. PFA bio-based resin has been attracting massive attention in recent years because of its low cost, polar structure, and high compatibility with hydrophilic nanoparticles. Several studies on the PFA resin pot life, curing kinetics, thermal treatment can be found [11-14] and are subjects of great interest. In this sense, due to the great importance of obtaining the PFA resin with uniform quality, our group has already worked on the optimization of PFA resin synthesis to assist in the porous carbon manufacture [15, 16].

Non-covalent approaches to produce carbon nanomaterial/polymer composites have been used due to their easy operation to synthesize them without changing the chemical structures of the constituent materials by a mixing process [17]. Also, this is a way to keep the intrinsic filler properties such as high electrical conductivity, optical properties, and mechanical strength. Thus, the driving forces to keep carbon nanomaterials and polymer molecules bonded are weak intermolecular forces including π-π interactions and electrostatic attractions [18-20].

Keeping in mind the above considerations, the production and characterization of carbon-polymer porous composites from a mixture of expanded graphite addition on furfuryl resin were studied. Firstly, the appropriate EG was produced by monitoring the time and temperature of intercalated graphite thermal expansion and characterized by field-emission gun scanning electron microscopy, Raman spectroscopy, and X-ray diffraction. After PFA processing, different EG amounts of 0.2, 0.5, and 1.0 wt% were ultrasonically dispersed in PFA resin. Modified PFA-EG resins were characterized by viscosimetry, differential scanning calorimetry (DSC), thermogravimetric analyses (TGA), and Fourier transform infrared spectroscopy (FTIR).

2. MATERIALS AND METHODS

2.1 Expanded graphite (EG)

EG was obtained from intercalated graphite (IG) Grafexp 95200-110, provided by Nacional de Grafite LTDA. The intercalated graphite was expanded by thermal treatment in a muffle for 10, 15, and 20 min at 500 °C. IG and EG images were obtained using a field emission gun scanning electron microscopy (FEG-SEM) Tescan Mira 3. Raman spectra were carried out from a LabRAM HR evolution Horiba Scientific equipment using 514.5 nm argon laser beam. X-ray diffractograms were obtained from PANanalytical model X'Pert Pro MPD diffractometer with CuK radiation.

2.2 Synthesis of poly(furfuryl alcohol)

The synthesis of PFA resin was carried out in a 2000 mL three-necked round-bottom flask, water bath at 32 °C, magnetic stirring, and a reflux system. 600 mL of distilled furfuryl alcohol was heated until 32 °C. Then, 85 mL of 0.5 mol L^{-1} sulfuric acid solution (P.A. FMaia reagent, 95-98%) was added as a catalyst. The reaction was controlled not exceed 60 °C, due to the reaction exothermy. After 1 h reation time, the PFA resin was obtained with viscosity of 300 mPa.s and subsequently neutralized until pH 5 value by adding concentrated sodium hydroxide solution (2 mol L^{-1}) directly on the resin. This pH value was considered suitable to minimize continuous polymerization improving carbon microstructure [21]. The resin was distilled on a rotary evaporator to reduce its moisture up to 2%. The moisture content was determined after resin distillation using a Karl Fischer Titrino plus 870 titrators from Metrohm Pensalab.

Viscosity control of PFA and PFA with 0.2, 0.5, and 1.0 wt% of EG additions was analyzed by using a Brookfield viscometer, model RV DV-II + Pro, spindle SC4-27. Modified PFA resins with different EG amounts were characterized by thermal analyses using a pressurized differential scanning calorimetry (PDSC) from TA Instruments DSC 2910, at a heating rate of 10 °C min^{-1}, in a temperature range from 30 to 250 ºC, under nitrogen pressure of 2.1 MPa. PFA and PFA_EG cured samples were analyzed by thermogravimetry in a Seiko equipment, model TG/DTA 6200, at a heating rate of 10 °C min^{-1} and under constant nitrogen flow (100 mL min^{-1}) with a temperature ranging from 25 to 1000 °C.

2.3 Processing of carbon-polymer porous composite

EG additions of 0.2, 0.5, and 1.0 wt% were dispersed in PFA resin using an ultrasonic tip for 30 min. Polyurethane foams with 70 pores per inch were impregnated with PFA and PFA_EG resins catalyzed by the addition of 3% (w/w) of p-toluenesulfonic acid aqueous solution (p-TSA; 60% w/v). The impregnated foams were cured in an oven for 1h in each threshold temperatures of 50, 70, 90, 110, and 130 ºC. The morphology of cured samples was evaluated by FEG-SEM from Tescan Mira3 after metal coating.

3. RESULTS AND DISCUSSION

3.1. EG preparation and characterization

The more appropriate expansion condition from IG to EG was achieved by varying different thermal expansion times. This procedure followed the paper of Gulnura et al. which optimized the heat treatment in muffle for IG expansion at 500 °C, starting from the natural graphitic material added with metallic particles [22]. Therefore, we studied the IG expansion at 500 ºC for 10, 15, and 20 min. The expansion time choice was based on the obtained results by physical and observable characterizations, such as mass loss and apparent volume (not shown). In this work it was observed that the thermal expansion reaction resulted in an apparent volume 5 times greater for all times, in comparison to that of starting material (IG) and weight loss up to 20%. This behavior can be explained by the intercalant decomposition from the starting material.

IG and EG SEM images for different thermal expansion times of 10, 15, and 20 min are shown in Figure 1 (A-D), respectively. The images depict that the expansion process promotes a larger surface area in these structures, and consequently, a possible reaction area where the graphene sheets are more exposed. In fact, the thermal expansion technique allows visualizing morphological changes from IG to EG, also observed by SENGUPTA *et al.* [23]. From images (A) to (D) a graphene cluster of IG packaged layer assembly was expanded by thermal treatment in short times. During the heat treatment, its intercalating component (in general sulfuric acid) is eliminated at 500 ºC resulting in an increase in the vertical spacing among these graphene planes of IG flake. The additional images (insets) show each morphology at higher magnification, allowing the expanded flake to be well observed. EG obtained for 10 min is not very expanded, clearly observed in the inset of Figure 1B. On the other hand, for EG 20 min the graphene layers were open, but a strong surface etching occurred defined as a deep hole in the image D. In fact, image (C) depicts a suitable morphology, obtained at 15 min with uniform and homogeneous open graphene sheets like an accordion carbon foam. This microstructure basically defines a honeycomb planar network. Therefore, EG obtained at 15 min was chosen as a filler of the polymeric matrix.

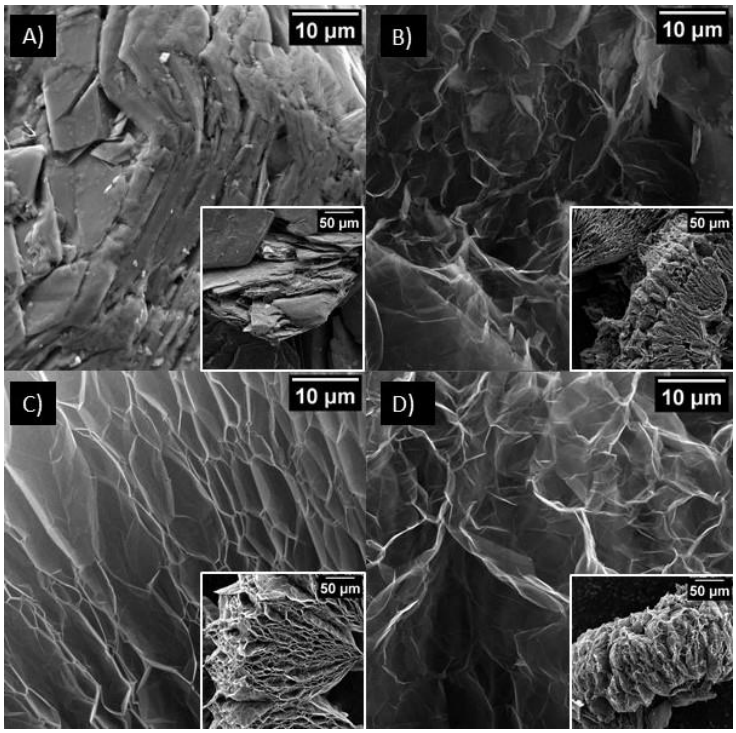

Figure 1: FEG-SEM images of IG (A) and EG obtained at (B) 10; (C) 15, and (D) 20 min.

The structural analyzes were accomplished by Raman and XRD spectra. IG and EG first and second-order Raman spectra are shown in Figure 2. The first-order spectra from 500 to 2000 cm^{-1} are characterized by D and G bands at around 1350 and 1580 cm^{-1}, respectively. G band is present in every form of sp^2 connection regarding the C = C bonds and it is originated from this bond stretching, which is a criterion for graphitic material identification [24]. On the other hand, D band is caused by the material structure disorder [24]. Also observing the first-order region, D' band presence at around 1600 cm^{-1} is noticeable, which is a little more defined in the EG spectrum, also induced by the disorder [25]. G band definition reflects an organized structure and it is coincident for IG and EG samples, suggesting that the treatment at 500 ºC did not modify their structure.

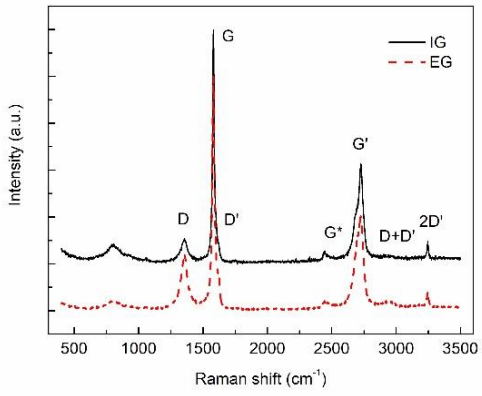

Figure 2: First and second-order Raman spectra of EG and IG.

In the second-order spectra from 2000 to 3500 cm^{-1}, G* and G' bands, located approximately at 2430 and 2720 cm^{-1}, respectively, were also identified [24]. G' band refers to a double resonance, attributed to the breathing mode of sp^2 aromatic rings. This band is related to the stacking of graphene sheets and for EG sample it is slightly displaced concerning the graphene Raman (2700 cm^{-1}), which may suggest that there is less interaction between two subsequent carbon layers, since EG looks like a spaced multilayer structure. Also, bands at 2900 and 3250 cm^{-1} are related to D+D' and 2D', respectively. Both are associated with disordered

structures and D+D' presents only a small contribution better observed in EG spectrum. Summarizing, no significant changes can be observed between IG and EG Raman features, except for G' that may be associated with two components for graphite structures [26].

X-ray diffraction is used as an important structural analysis for carbon materials as it considers a large sample volume. IG and EG XRD patterns present the peaks at 2θ = 26.5 ° and 54.6 ° which represent the crystalline phase of (002) and (004), respectively, already discussed by other authors [27, 28], characteristic of graphitic material as shown in Figure 3. Also, the phase (100) at 2θ = 42 ° was observed. The interplanar distance (d002) was calculated from Bragg's Law while the pilling up width (Lc) and crystallite size (La) were also evaluated from the Scherrer formula [29]. The calculations were performed by pattern deconvolutions according to Manoj and Kunjomana (2012) [30] and they are presented in Table 1 for IG and EG samples. The Lc values were 12.15 and 15.55 nm for IG and EG, respectively, which show an increase in the stacking of graphene sheets for EG. This Lc increase may be related to the elimination of intercalating compounds, which in high concentrations cause a steric resistance between two subsequent graphene sheets and make the stacking more difficult [31]. The interplanar distance between the graphene sheets, calculated for both materials, was 0.338 nm and it is in accordance with the theoretically expected value and with that observed by other authors [32, 33].

These results suggest that the IG heat treatment to produce EG did not change the structure among the layers. However, for the crystallite size a decrease occurred from 51.91 to 18.95 nm with the IG expansion. This behavior can be attributed to the breakdown of the graphene planes during the heating process. Nonetheless, due to the peak at 26.6º appearance for both samples, it is estimated that the structure remained in its minimum configuration and that the carbon crystal did not change.

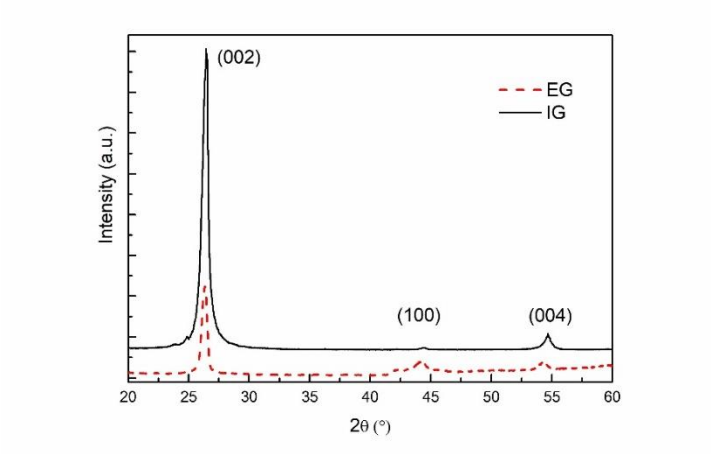

Figure 3: First and second-order Raman spectra of EG and IG.

Table 1: Results obtained from IG and EG XRD patterns.

XRD	2θ (002)	2θ (100)	d_{002} (nm)	Lc (nm)	La (nm)
IG	26.40	42.27	0.34	12.15	51.91
EG	26.40	42.34	0.34	15.55	18.95

3.2. PFA resin with different EG amounts: production and characterization

PFA resin synthesis requires a controlled furfuryl alcohol polymerization reaction due to its exothermic process. Taking into account the methodology used in previous study related to this reaction [21], PFA resin was obtained with pH ~5, moisture content of around 2%, and viscosity around 300 mPa.s. This viscosity value is required for making easier the filler dispersion as well as the material impregnation on PU foam. In this context, Y. Li et al. have reported that when carbon nanotubes are used as filler on polymer matrix their content was controlled up to 10 wt% due to a significant viscosity increase, which leads to the poor processability and inferior quality of the final composite material [1]. Thus, purity, integrity, content, filler dispersion in addition to polymer type can be pointed out as critical factors that influence the composite properties, such as their electrical and mechanical performances.

The more appropriated processing parameters of the resin cure are supported by its thermal and rheological behaviors and are related to physical-chemical resin characteristics. Among them, viscosity is an im-

portant parameter because its suitable control facilitates the volatile release and favors an efficient PU impregnation. Regarding a rheological study of PFA resin with different EG amounts Figure 4 shows the viscosity variation as a function of the temperature increase using p-TSA catalyst for PFA resin composites. As expected, the resin viscosity value increased with the EG addition increase, but presented similar profiles. Nonetheless, for the sample preparations, the resin fluidity was kept suitable in this EG addition range, which was very important for the posteriori PU foam impregnation. For 1.0 wt% addition, the viscosity profile presented a considerable change, where T(gel) was anticipated and at this point the viscosity value increased at around 50%. This can also be seen in Table 2 analyzing the reduced crosslinking time by comparing PFA_1% EG and pure PFA. This performance indicated that small EG addition caused fast polymeric chain increase at which the polymer became solid and no longer flows resulted in a crosslinking process. Considering this approach, J.M. Sadler et al. have discussed that the dominating factor for crosslinking and molecule weight increase for PFA is the chain branching formation [34]. Viscosity increases is related to the increase of molecular weight. However, once the concentration of oligomer reaches a critical point, chain branching occurs rapidly increasing the resin viscosity. This factor may be related to the EG addition as solid dispersed nanoparticles in the resin forming a network among them which may facilitate the branch pathway when alternative structures are formed. This behavior is clear because in the heating range studied the resin gelification became faster and faster as the EG addition increased. Table 2 shows the viscosity, where the samples were analyzed at 27ºC to determine the initial viscosity values, T(gel), and total time to reach T(gel) values for resins with different EG wt%, considering the heating rate used of 2.0 °C/min. This performance is confirmed by the analysis of the region of minimum viscosity that was also altered. From 35 to 41 ºC, the EG presence gently shifts the minimum viscosity value, where the minimum of pure PFA sample is at 40.97 ºC with a viscosity value of 270 mPa.s. The subsequent values are: for 0.2% EG from 36.90 to 38.90 ºC (300 mPa.s), for 0.5% EG from 37.02 to 40.01ºC (347.5 mPa.s), and for 1.0% EG from 35.02 to 35.50ºC (497.5 mPa.s). This fact is a significant indicator to favor the resin impregnation in its matrix foam in addition to the anticipation of the curing process, as shown in the Table 2, keeping a good dispersion over the matrix, even for a sample with 1.0% EG.

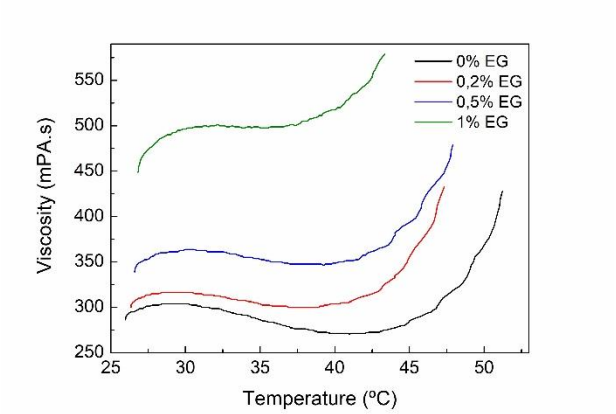

Figure 4: Viscosity variation vs. increasing the temperature of the PFA resin with different amounts of EG.

Table 2: Viscosity and gel temperature of PFA resin with different percentages of EG.

PFA_%EG	Ƞ (mPa.s)	T gel(°C)	Time (min)
0	303	45.41	11.21
0.2	313	42.89	9.92
0.5	356	43.55	9.93
1.0	468	38.84	7.32

PDSC technique was used in this work in order to evaluate the cure behavior of PFA resin. PDSC thermograms of PFA resin prepared with *p*-TSA catalyst at 3 wt% at heating rates of 10 °C/min, are displayed in Figure 5. In general, all curves present an exothermic peak with a weak endothermic peak in the range of 130–180 °C that was associated with water evolved from the condensation reaction [35]. Nonetheless, the higher the EG addition the lower the T*onset* and T*endset*, as expected. This behavior corroborates with the viscosity measurement results. Also, can be observed a small variation concerning the thermal behavior involving neat resin and the PFA resin with EG, showing that the cure kinetics probably is modified

with the adding of EG.

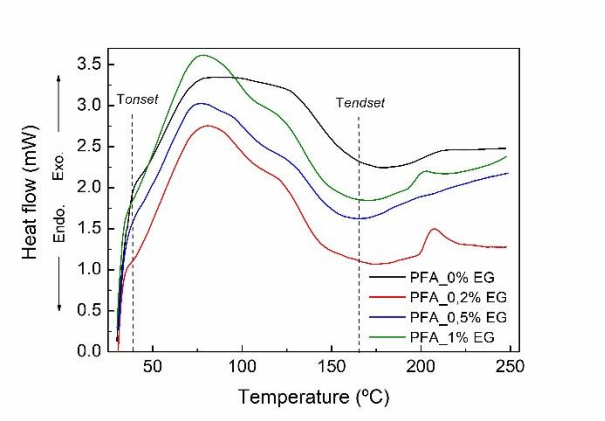

Figure 5: Results of the PDSC of furfuryl resin with different percentages of EG.

In fact, before discussing some specific features of each thermogram, some assumptions related to these EG filler properties must be highlighted. Firstly, EG was obtained by thermal treatment in air atmosphere which probably introduced oxygen-containing functional groups increasing its hydrophilic behavior. Thus, the oxygen-functional groups are important for the curing process in these carbon-polymer composites. M.A. VARGAS-HERNADEZ *et al.* [35] have discussed that when GO was used as filler in PFA resin the higher the number of GO surface oxidized groups major catalytic activity was observed.

Table 3: Onset, peak, and endset temperatures variations of PFA resin with different percentages of EG.

Samples	**Tonset (°C)**	**Tpeak (°C)**	**Tendset (°C)**
PFA_0% EG	40.90	78.24	177.01
PFA_0.2%EG	39.45	80.83	174.63
PFA_0.5%EG	39.36	77.31	165.74
PFA_1%EG	38.05	78.80	168.37

From Figure 5 the curing of the neat resin presents a flatter peak and higher initial and final curing temperatures than those of PFA_EG composites where the first exothermic peak at around 77 °C was becoming narrower and more pronounced as the EG addition increased proving that even a small EG amount was significant to decrease the resin cure time with a minimal Tendset for PFA with 0.5 wt%, although this peak improved its definition, width, and height for EG 1.0 wt%. This behavior may be related to the presence of oxygen-functional groups on the EG surface to promote faster reactions, consistent with strong matrix–particle interactions. Table 3 shows Tonset, Tpeak, and Tendset variations from PDSC curves.

After characterizing the PFA resins with different EG percentages the PU foams were impregnated with them using p-TSA catalyst at 3 wt% to be submitted to the curing process, as described in the methodology. The thermogravimetric analysis allows us to know the mass loss behavior of the resin with the different EG addition when this material is exposed to temperature. These measurements were obtained for PFA and PFA_EG composites impregnated on PU foam after cure process. The weight loss and derivative weight results for the sample set are shown in Figure 6. In a general view, for the degradation, the EG increase did not change the mass loss profile in a drastic way. At 900 °C, a small variation with respect to the residual mass was observed from 54.4% (pure resin) to 55.7% (EG 0.2 wt%).

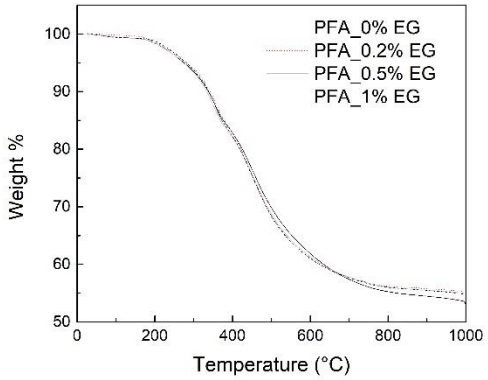

Figure 6: TGA results of PFA_EG composites.

In order to assess the functional groups presented in IG and EG, the FTIR technique was applied as a complement to study these graphitic materials, since it provides information on the interactions between molecules or atoms through magnetic radiation by a process of molecular vibration. Both IG and EG spectra are shown in Figure 7 with an enlarged region from 2200 to 3600 cm^{-1} for EG, which is a characteristic stretch region attribute to carboxyl bonds (RCOOH) [36]. Besides being a region where hydroxyl stretching would be present, its peaks are superimposed. The broadband at around 3400 cm^{-1} for the hydroxyl indicates the presence of oxygen containing, such as carbonyl, carboxylic, epoxy, and hydroxyl groups [37]. Peaks at 2922 and 2840 cm^{-1} are attributed to methane [38, 39] and are present in both samples, as well as the peaks of 1582 and 1622 cm^{-1} slightly offset from 1580 and 1636 cm^{-1} are present, but they are not well defined [39, 40]. Knowing that each organic function presents in the spectrum is in the range from 900 to 1300 cm^{-1}, the similarity of the two samples of IG and EG is clear taking in mind that the original carbon structure was maintained for both. Also, the peak at 1067cm^{-1} is slightly offset to 1054 cm^{-1} and represent C-O stretching vibrations while 1240 cm^{-1} is assigned to C-OH stretch, also found in graphite oxides [41].

Considering the cured PFA and PFA_EG composites the FTIR technique was applied as additional information related to their functional groups. Figure 7 presents FTIR spectra of cured PFA and cured PFA_EG composites. The spectra show intense peaks at ~ 2862 and 2923 cm^{-1} that are attributed to symmetry and asymmetry CH_2 stretching [10]. Other considered bands are: 784, 1011, 1615 and 3120 cm^{-1}, corresponding to–C = C– and = C - O - C =, characteristics of the furan group of furfuryl alcohol as a resin precursor. A band at 1714 cm^{-1} can be attributed to the ring rupture during the curing process [21], whereas an aliphatic resin chain appears in the band at 2923 cm^{-1}. Some bands are superimposed by others or appear more prominently in the resin spectrum, such as 1120 cm^{-1}, attributed to C-O or C-OH band stretching [21, 39]. Other important peaks are depicted in Table 4.

In view of the different EG wt% additions the spectra show significant variations in the region from 650 to 859 cm^{-1}, where the peak intensity is relatively reduced in cured PFA_EG samples. Bearing in mind that the peak at 784 cm^{-1} is related to the C = C bonds of the furan ring, EG may interact with the resin structure, replacing the double bond. In the region from 900 to 1250 cm^{-1}, the lower peak intensity is also noticed when comparing the pure resin with samples containing EG. The peak at 1154 cm^{-1}, related to the C-O graphite stretch [42], has the lowest energy to be observed in FTIR and its signal decreased for PFA_EG 1 wt%. From 1500 to1750 cm^{-1}, a significant peak is observed at 1554 cm^{-1}, characteristic of the C = C vibration, which appears due to the interconnection of a furan-CH_2-furan group by a condensation reaction, which is in agreement with the polymerization process, being more intense in the pure PFA sample [43, 44].

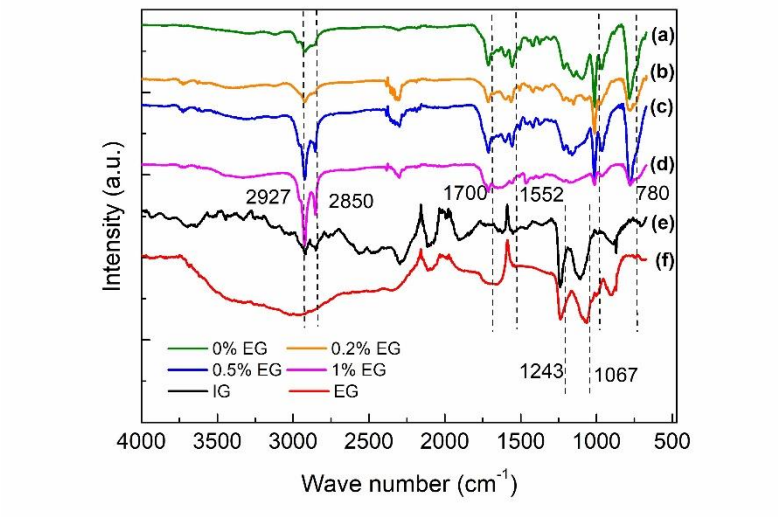

Figure 7: FT-IR spectra of IG, EG and cured PFA with EG additions.

The peaks at 2922 and 2858 cm^{-1} can be attributed to the intense vibrations of the methane group directly related to the graphitic component, explaining its better definition for the sample with 1.0 wt% EG [38]. According to Goudarzi et al., EG shows a peak at 1620 cm^{-1} referring to the carboxyl functional group, like 780cm^{-1}, present at the edges of the modified graphite [40, 45]. The furan ring vibration at 780 cm^{-1} can be indicative of 2-mono substitution on the furan ring [45]. It appeared with a small shift displaced and low intensity at 1613 cm^{-1} [38, 40, 43]. The region around this peak, at 1270 and at 1795 cm^{-1} shows a transmittance intensity reduction when we compare the PFA spectrum with those of PFA_EG composites. The peak at 1460 cm^{-1} becomes present only in the sample with 1.0 wt % EG and is related to the symmetrical stretching of the C-C-C carbon chain, which suggests that the sample with the highest EG content may be more organized, since EG Raman spectrum presented a high carbon ordering higher than that of IG. A comparison of peaks found in each sample studied can be seen in the Table 5. However, no sharp differences were observed in the analyzed spectra, which may be related to the low concentration of the reinforcement in the matrix. In addition, the intensities of the graphite molecule vibrations are less pronounced in FTIR compared to those of PFA resin, due to the dipole of the typical aromatic ring bonds in the graphitic material. This effected also influenced the decrease in peak intensities in the spectra as the EG amount increased in the PFA_EG composites.

Table 4: FTIR bands attribution to IG, EG, and cured samples of PFA and PFA_EG composites.

IG	EG	PFA	PFA 0.2%EG	PFA 0.5%EG	PFA 1% EG	Peak	Assignments	Ref
		785	783	782	779	788	-C=C- connections	[21]
868	900	1016	1014	1014	1014	1008	Isopropyl group	[46, 47]
1102	1070	1151	1155	1157	1178	1154	Elongation of C-O	[39, 42]
1243	1243	1222	1214	1218	1214	1220	C-O alcohol or C-O-C of the furan ring	[21]
		1311				1295	Deformation of aromatic rings	[48]
1350		1376	1354	1374	1377	1360	Stretch C-C or CO	[21]
		1417	1421	1417	1419	1430	Aliphatic tracking	[10, 21]
1552	1529	1500	1506	1507	1466	1506	Carboxyl groups and Axial deformation of the furan ring	[21, 39, 48]
1613		1557	1564	1555	1555	1565	Elongation of C=C in the aromatic ring	[38, 40, 43]
1897	1715	1712	1712	1715	1711	1715	C=O of carboxylic acid	[21, 46, 47]

							and rupture of the furan ring	
		2852	2866	2851	2853	2850	Enlongation of CH_2	[49]
		2928	2929	2924	2924	2920	Enlongation of CH_3 and aliphatic chain	[49]
2840		2976		2962	2959	2963	Stretch C-H	[39, 48]

Figure 8 shows SEM images of impregnated foams with neat PFA and PFA_EG 1 wt% after cure. The homogeneous impregnation even after EG addition is clear, as a result of the suitable viscosity with good fluidity. The inset shows the stem surface with higher magnification where EG presence can be associated with the surface roughness, while the surface of neat PFA is smoother. These images show that EG can be considered a good filler for the production of porous composites and can be easily dispersed with amounts up to 1.0 wt%.

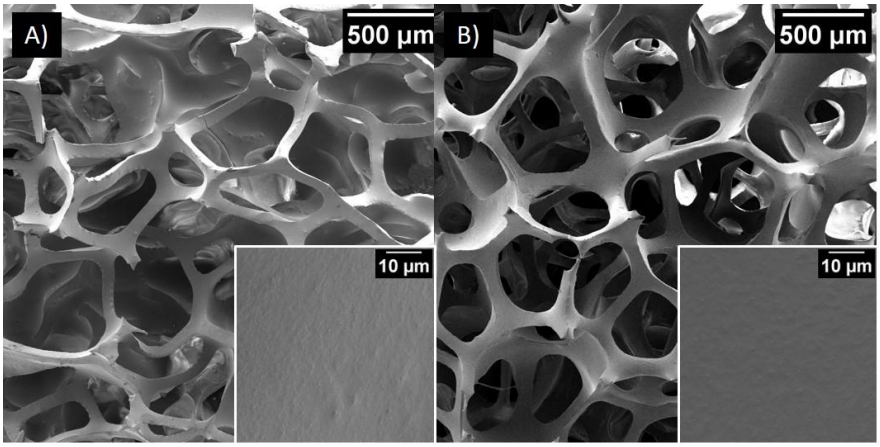

Figure 8: FEG-SEM images of impregnated foams with (A) neat PFA and (B) PFA_EG 1 wt% after cure.

4. CONCLUSION

Carbon-polymer porous composite was produced and characterized with success. EG filler and PFA constituent materials were explored taking into account their suitable proportion to optimize the composite processing assured by their morphological and structural characterizations. The addition of up to 1.0 wt% of EG kept the resin fluidity not drastically altering the viscosity which contributed to an appropriated impregnation of the polyurethane foams. Viscosimetric and differential scanning calorimetry techniques showed that EG addition contributed to the crosslinking formation, decreasing the onset and endset temperatures due to the presence of functional groups on its surface that acted as catalysts. FTIR analyses confirmed the presence of functional groups on IG and EG. On the other hand, the thermogravimetric analysis did not show any significant changes caused by EG addition.

5. ACKNOWLEDGMENTS

The authors acknowledge the Brazilian agencies São Paulo Research Foundation (FAPESP grant # 2017/10118-0), CAPES and CNPq (grant # 132316/2018-8 and grant # 303224/2016-9) for the financial support and Nacional de Grafite for supplying the intercalated graphite.

6. BIBLIOGRAPHY

[1] LI, Y., HUANG, X., ZENG, L., *et al.*, *A review of the electrical and mechanical properties of carbon nanofiller-reinforced polymer composites*, Journal of Materials Science, v. 54, n. 2, pp. 1036-1076, Jan. 2019.

[2] MILLER, S. G., BAUER, J.L., MARYANSKI, M. J., *et al.*, *Characterization of epoxy functionalized graphite*

nanoparticles and the physical properties of epoxy matrix nanocomposites, Composites Science and Technology, v. 70, n. 7, pp. 1120-1125, Jul. 2010.

[3] NOH, Y. J., KIM, H. S., KU, B.-C., *et al.*, *Thermal Conductivity of Polymer Composites With Geometric Characteristics of Carbon Allotropes*, Advanced Engineering Materials, v. 18, n. 7, pp. 1127-1132, Jul. 2016.

[4] ZHENG, W., QI, T., ZHANG, Y. C., *et al.*, *Fabrication and characterization of a multi-walled carbon nanotube-based counter electrode for dye-sensitized solar cells*, Xinxing Tan Cailiao/New Carbon Materials, v. 30, n. 5, pp. 391-396, 2015.

[5] POKHAREL, P., XIAO, D., EROGBOGBO, F., *et al.*, *A hierarchical approach for creating electrically conductive network structure in polyurethane nanocomposites using a hybrid of graphene nanoplatelets, carbon black and multi-walled carbon nanotubes*, Composites Part B: Engineering, v. 161, pp. 169-182, Mar. 2019.

[6] CHUNG, D. D. L., *A review of exfoliated graphite*, Journal of Materials Science, v. 51, n. 1, pp. 554-568, 2015.

[7] SANSEVERO, A. C., RUDDY, Y., *Carbon-Containing Polymer Composites*, v. 16, n. 5, Singapore, Springer Singapore, 2019.

[8] YIM, Y. J., PARK, S.J., *Effect of silver-plated expanded graphite addition on thermal and electrical conductivities of epoxy composites in the presence of graphite and copper*, Composites Part A: Applied Science and Manufacturing, v. 123, n. June 2018, pp. 253-259, 2019.

[9] ZHANG, Y., PARK, S. J., *Imidazolium-optimized conductive interfaces in multilayer graphene nanoplatelet/epoxy composites for thermal management applications and electroactive devices*, Polymer, v. 168, n. January, pp. 53-60, 2019.

[10] MONTAGNA, L. S., OISHI, S. S., DINIZ, M. F., *et al.*, *Multifunctional green nanostructured composites: preparation and characterization*, Materials Research Express, v. 5, n. 5, p. 055010, May 2018.

[11] MAREFAT SEYEDLAR, R., IMANI, M., MIRABEDINI, S. M., *Curing of poly(furfuryl alcohol) resin catalyzed by a homologous series of dicarboxylic acid catalysts: Kinetics and pot life*, Journal of Applied Polymer Science, v. 133, n. 43, Nov. 2016.

[12] DIAS, F. da S., BRAZIL, T. R., MONTAGNA, L. S., *et al.*, *Estudo da influência dos parâmetros de tratamento térmico da resina furfurílica nas características morfológicas, estruturais e condutividade elétrica do carbono vítreo reticulado*, Matéria (Rio de Janeiro), v. 26, n. 2, 2021.

[13] DOMÍNGUEZ, J. C., GRIVEL, J. C., MADSEN, B., *Study on the non-isothermal curing kinetics of a polyfurfuryl alcohol bioresin by DSC using different amounts of catalyst*, Thermochimica Acta, v. 529, pp. 29-35, 2012.

[14] ORIGO, F. D., ARISSETO, J. C., SEIXAS, F. L., *et al.*, *Acid catalyst influence on the polymerization time of polyfurfuryl alcohol and on the porosity of monolithic vitreous carbon*, Journal of Applied Polymer Science, v. 133, n. 20, 2016.

[15] OISHI, S. S., REZENDE, M. C., ORIGO, F. D., *et al.*, *Viscosity, pH, and moisture effect in the porosity of poly(furfuryl alcohol)*, Journal of Applied Polymer Science, v. 128, n. 3, pp. 1680-1686, 2013.

[16] OISHI, S. S., BOTELHO, E. C., REZENDE, M. C., *et al.*, *Structural and surface functionality changes in reticulated vitreous carbon produced from poly(furfuryl alcohol) with sodium hydroxide additions*, Applied Surface Science, v. 394, pp. 87-97, 2017.

[17] MENG, D., FAN, J., MA, J., *et al.*, *The preparation and functional applications of carbon nanomaterial/conjugated polymer composites*, Composites Communications, v. 12, n. December 2018, pp. 64-73, 2019.

[18] GENG, J., ZENG, T., *Influence of single-walled carbon nanotubes induced crystallinity enhancement and morphology change on polymer photovoltaic devices*, Journal of the American Chemical Society, v. 128, n. 51, pp. 16827-16833, 2006.

[19] PRESTO, D., SONG, V., BOUCHER, D., *P3HT/graphene composites synthesized using In situ GRIM methods*, Journal of Polymer Science, Part B: Polymer Physics, v. 55, n. 1, pp. 60-76, 2017.

[20] SUN, J., XIAO, L., MENG, D., *et al.*, *Enhanced photoresponse of large-sized photoactive graphene composite films based on water-soluble conjugated polymers*, Chemical Communications, v. 49, n. 49, pp. 5538-5540, 2013.

[21] OISHI, S. S., BOTELHO, E. C., REZENDE, M. C., *et al.*, *Structural and surface functionality changes in reticulated vitreous carbon produced from poly(furfuryl alcohol) with sodium hydroxide additions*, Applied Surface Science, v. 394, pp. 87-97, Feb. 2017.

[22] GULNURA, N., KENES, K., YERDOS, O., *et al.*, *Preparation of Expanded Graphite Using a Thermal Method*, IOP Conference Series: Materials Science and Engineering, v. 323, n. 1, 2018.

[23] SENGUPTA, R., BHATTACHARYA, M., BANDYOPADHYAY, S., *et al.*, *A review on the mechanical and electrical properties of graphite and modified graphite reinforced polymer composites*, Progress in Polymer Science (Oxford), v. 36, n. 5, pp. 638-670, 2011.

[24] MALARD, L. M., PIMENTA, M. A., DRESSELHAUS, G., *et al.*, *Raman spectroscopy in graphene*, Physics Reports, v. 473, n. 5-6, pp. 51-87, 2009.

[25] CANÇADO, L. G., JORIO, A., PIMENTA, M. A., *Measuring the absolute Raman cross section of nanographites as a function of laser energy and crystallite size*, Physical Review B - Condensed Matter and Materials Physics, v. 76, n. 6, pp. 1-7, 2007.

[26] FERRARI, A. C., *Raman spectroscopy of graphene and graphite: Disorder, electron–phonon coupling, doping and nonadiabatic effects*, Solid State Communications, v. 143, n. 1–2, pp. 47–57, 2007.
[27] DEBELAK, B., LAFDI, K., *Use of exfoliated graphite filler to enhance polymer physical properties*, Carbon, v. 45, n. 9, pp. 1727-1734, 2007.
[28] ZENG, J. L., CHEN, Y. H., SHU, L., *et al.*, *Preparation and thermal properties of exfoliated graphite/erythritol/mannitol eutectic composite as form-stable phase change material for thermal energy storage*, Solar Energy Materials and Solar Cells, v. 178, n. August 2017, pp. 84-90, 2018.
[29] TAKAI, K., OGA, M., SATO, H., *et al.*, *Structure and electronic properties of a nongraphitic disordered carbon system and its heat-treatment effects*, Physical Review B, v. 67, n. 21, pp. 1-11, 2003.
[30] MANOJ, B., KUNJOMANA, A. G., *Study of stacking structure of amorphous carbon by X-ray diffraction technique*, International Journal of Electrochemical Science, v. 7, n. 4, pp. 3127-3134, 2012.
[31] COLLINS, J., ZHENG, D., NGO, T., *et al.*, *Partial graphitization of activated carbon by surface acidification*, Carbon, v. 79, pp. 500–-517, 2014.
[32] CUESTA, A., DHAMELINCOURT, P., LAUREYNS, J., *et al.*, *Comparative performance of X-ray diffraction and Raman microprobe techniques for the study of carbon materials*, Journal of Materials Chemistry, v. 8, n. 12, pp. 2875-2879, 1998.
[33] BADENHORST, H., *Microstructure of natural graphite flakes revealed by oxidation: Limitations of XRD and Raman techniques for crystallinity estimates*, Carbon, v. 66, pp. 674-90, Jan. 2014.
[34] SADLER, J. M., YEH, I.-C., TOULAN, F. R., *et al.*, *Kinetics studies and characterization of poly(furfuryl alcohol) for use as bio-based furan novolacs*, Journal of Applied Polymer Science, v. 135, n. 34, p. 46608, Sep. 2018.
[35] VARGAS-HERNÁNDEZ, M. Á., SULBARÁN-RANGEL, B., VÁZQUEZ-TORRES, H., *Non-isothermal curing kinetics of biocomposite from poly(furfuryl alcohol) and graphene oxide or reduced graphene oxide with different contents of oxygen-groups by DSC*, Thermochimica Acta, v. 684, p. 178485, Feb. 2020.
[36] CHEN, X., WANG, X., WANG, S., *et al.*, *Furfuryl alcohol functionalized graphene for sorption of radionuclides*, Arabian Journal of Chemistry, v. 10, n. 6, pp. 837-844, 2017.
[37] THAKUR, S., KARAK, N., *Multi-stimuli responsive smart elastomeric hyperbranched polyurethane/reduced graphene oxide nanocomposites*, J. Mater. Chem. A, v. 2, n. 36, pp. 14867-14875, 2014.
[38] LAN, R., SU, W., LI, J., *Preparation and Catalytic Performance of Expanded Graphite for Oxidation of Organic Pollutant*, Catalysts, v. 9, n. 3, p. 280, Mar. 2019.
[39] GÜLER, Ö., GÜLER, S. H., SELEN, V., *et al.*, *Production of graphene layer by liquid-phase exfoliation with low sonication power and sonication time from synthesized expanded graphite*, Fullerenes, Nanotubes and Carbon Nanostructures, v. 24, n. 2, pp. 123-127, Feb. 2016.
[40] GOUDARZI, R., HASHEMI MOTLAGH, G., *The effect of graphite intercalated compound particle size and exfoliation temperature on porosity and macromolecular diffusion in expanded graphite*, Heliyon, v. 5, n. 10, p. e02595, Oct. 2019.
[41] KARTICK, B., SRIVASTAVA, S. K., SRIVASTAVA, I., *Green Synthesis of Graphene*, Journal of Nanoscience and Nanotechnology, v. 13, n. 6, pp. 4320-4324, Jun. 2013.
[42] ROGHANI-MAMAQANI, H., HADDADI-ASL, V., MORTEZAEI, M., *et al.*, *Furfuryl alcohol functionalized graphene nanosheets for synthesis of high carbon yield novolak composites*, Journal of Applied Polymer Science, v. 131, n. 11, pp. 1-8, 2014.
[43] ZAVAGLIA, R., GUIGO, N., SBIRRAZZUOLI, N., *et al.*, *Complex kinetic pathway of furfuryl alcohol polymerization catalyzed by green montmorillonite clays*, Journal of Physical Chemistry B, v. 116, n. 28, pp. 8259-8268, 2012.
[44] HANIFPOUR, A., MIRAGHAIE, S., ZOHURIAAN-MEHR, M. J., *et al.*, *Poly(furfuryl alcohol) bioresin-modified LY5210 epoxy thermosets*, Journal of Polymer Research, v. 26, n. 8, p. 198, Aug. 2019.
[45] POPHALI, A., LEE, K.-M., ZHANG, L., *et al.*, *First synthesis of poly(furfuryl) alcohol precursor-based porous carbon beads as an efficient adsorbent for volatile organic compounds*, Chemical Engineering Journal, v. 373, n. January, pp. 365-374, Oct. 2019.
[46] FALCO, G., GUIGO, N., VINCENT, L., *et al.*, *Opening Furan for Tailoring Properties of Bio-based Poly(Furfuryl Alcohol) Thermoset*, ChemSusChem, v. 11, n. 11, pp. 1805-1812, Jun. 2018.
[47] DEKA, H., MISRA, M., MOHANTY, A., *Renewable resource based "all green composites" from kenaf biofiber and poly(furfuryl alcohol) bioresin*, Industrial Crops and Products, v. 41, n. 1, pp. 94-101, Jan. 2013.
[48] DA SILVA, D. D., DOS SANTOS, W. F., PEZZIN, S. H., *Nanocompósitos de matriz epoxídica com reforços produzidos a partir do grafite natural*, Revista Materia, v. 18, n. 2, pp. 1260-1272, 2013.
[49] LIU, X., RAO, Z., *Experimental study on the thermal performance of graphene and exfoliated graphite sheet for thermal energy storage phase change material*, Thermochimica Acta, v. 647, pp. 15-21, 2017.

ORCID

Raissa Samira Rocha da Silva https://orcid.org/0000-0002-0884-6567
Silvia Sizuka Oishi https://orcid.org/0000-0001-5540-3382
Luiza dos Santos Conejo https://orcid.org/0000-0001-5533-1374
Edson Cocchieri Botelho https://orcid.org/0000-0001-8338-4879
Neidenêi Gomes Ferreira https://orcid.org/0000-0002-3057-262X